Templated Synthesis of Uniform Perovskite Nanowire Arrays

Michael J. Ashley,[†,‡] Matthew N. O'Brien,[‡,§] Konrad R. Hedderick,[‡,∥] Jarad A. Mason,[‡,§] Michael B. Ross,[‡,§] and Chad A. Mirkin*,[†,‡,§,∥]

[†]Department of Chemical & Biological Engineering, [‡]International Institute for Nanotechnology, [§]Department of Chemistry, and [∥]Department of Materials Science & Engineering, Northwestern University, Evanston, Illinois 60208, United States

Ⓢ Supporting Information

ABSTRACT: While the chemical composition of semiconducting metal halide perovskites can be precisely controlled in thin films for photovoltaic devices, the synthesis of perovskite nanostructures with tunable dimensions and composition has not been realized. Here, we describe the templated synthesis of uniform perovskite nanowires with controlled diameter (50−200 nm). Importantly, by providing three examples ($CH_3NH_3PbI_3$, $CH_3NH_3PbBr_3$, and Cs_2SnI_6), we show that this process is composition general and results in oriented nanowire arrays on transparent conductive substrates.

Efficient visible light absorption and long charge carrier diffusion lengths make metal halide perovskites an appealing class of low-cost, solution-processable materials for next-generation solar cells and other optoelectronic devices.[1−6] Due to their ease of preparation and impressive performance, most investigations of perovskite materials have utilized thin film architectures modified in their chemical composition. More recently, several groups have attempted to synthesize perovskite nanowires[7] to further improve crystallinity[8−11] and charge extraction in photovoltaics.[12] From these early studies, it is apparent that syntheses integrating nanowires into device architectures should (1) maintain the ease of use and solution processability of thin film preparations, (2) produce uniform structures in contact with a transparent conductive electrode, and (3) orient nanowires within an inert scaffold to eliminate shunting pathways. Previous approaches to perovskite nanowire synthesis include antisolvent crystallization,[13,14] reaction of a solid metal salt with an organohalide solution,[8,15,16] and partial dissolution and recrystallization of a perovskite film.[12,17] While significant advances have been made, these methods often result in low yields of nanowires, typically as mixtures of rods, wires, plates, and aggregated spheres, with large variations in size.[8,9,13−15] To the best of our knowledge, the most uniform reported perovskite nanowires exhibit ∼20% variation in diameter with no control over average size.[18] These structural inhomogeneities preclude a systematic investigation of how nanoscale architecture impacts the optoelectronic properties and ultimately the device performance of perovskite nanomaterials.

To overcome these limitations, we employed anodized aluminum oxide (AAO) templates[19−21] with oriented, cylindrical nanopores to synthesize uniform perovskite nanowire arrays. AAO represents an ideal template for nanowire synthesis, because (1) it can be directly prepared on transparent conductive substrates for subsequent device integration, (2) pore diameter can be finely tuned to control nanowire diameter (D), and (3) the formation of spatially discrete, oriented nanowires enables systematic structure−function characterization. Traditionally, electrodeposition has been used to generate nanomaterials within AAO, including metals,[22−24] simple inorganic semiconductors,[20,24,25] and polymers.[23,24] However, many materials, such as metal halide perovskites, cannot be reliably electrodeposited in a single step.[26] This necessitates the development of an alternative method in which AAO can serve as a template for the formation of perovskite nanowires.

Here, a perovskite precursor solution is added to an AAO template, followed by dissolution and recrystallization of the material. Using this technique, large-area perovskite nanowire arrays can be synthesized with D dictated by the AAO pore diameter (from 50 to 200 nm). By virtue of the template used, this results in nanowires oriented perpendicular to a transparent conductive electrode (TiO_2/fluorine-doped tin oxide (FTO) glass). Importantly, we demonstrate that this process is composition general and can be used to synthesize organometal halide perovskite ($CH_3NH_3PbI_3$ and $CH_3NH_3PbBr_3$) and all-inorganic perovskite (Cs_2SnI_6) nanowires. X-ray diffraction (XRD) shows that crystal quality depends on diameter and correlates well with time-resolved photoluminescence (PL) spectroscopy measurements.

In a typical experiment, a layer of TiO_2 was deposited onto FTO glass according to literature methods.[27] Aluminum was then evaporated onto these substrates, followed by anodization to induce nanopore formation. In this process, the applied anodization voltage dictates the interpore spacing.[21,25] A subsequent pore refinement step[23] results in uniform pore diameters and dissolves the barrier layer at the bottom of each pore.[25] To form $CH_3NH_3PbI_3$ nanowires in these templates, a $CH_3NH_3PbI_3$ precursor solution in dimethylformamide (DMF) was added and allowed to penetrate the pores of AAO, followed by removal of excess liquid from the template surface and annealing (Figure 1a-I). While this step results in crystalline perovskite nanowires, solvent evaporation from the AAO surface during annealing led to material contraction such that much of the perovskite material within the template did not touch the bottoms of the pores. Additionally, a thin perovskite film remained on the surface of the AAO.
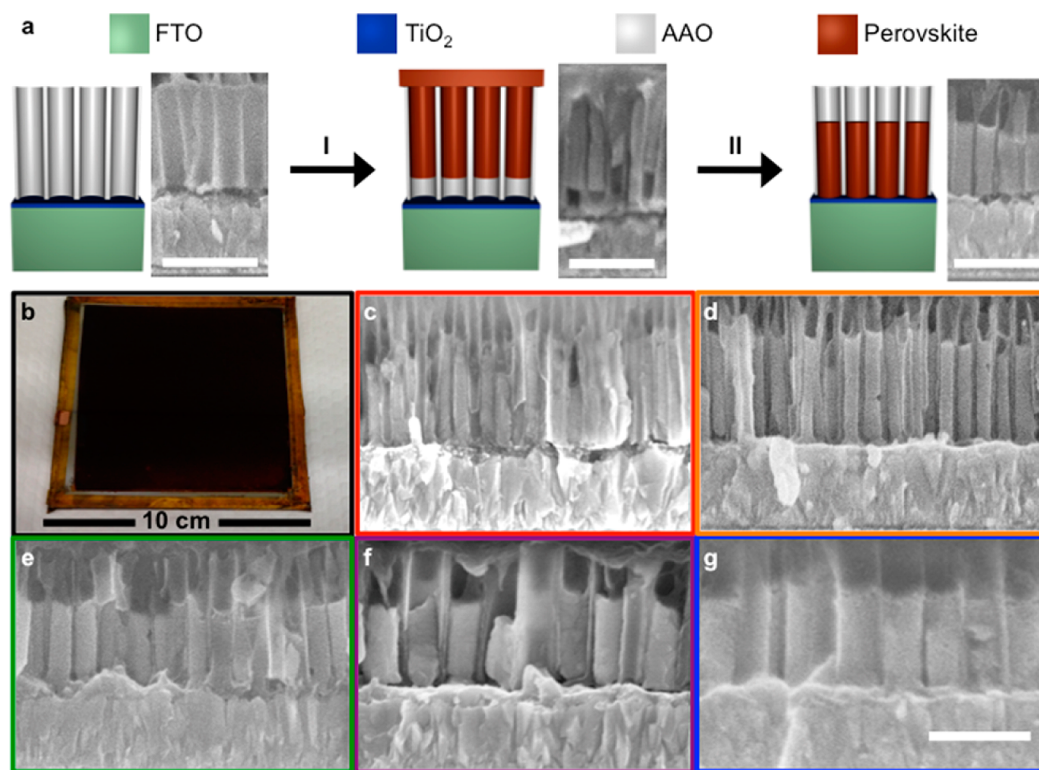
Figure 1. Synthesis of perovskite nanowire arrays in AAO. (a) $CH_3NH_3PbI_3$ precursor solution penetrates the AAO pores, followed by spin coating and annealing (I). Sample is exposed to a DMSO/chlorobenzene solution followed by a short annealing step (II). (b) Photograph of a ∼9 × 9 cm nanowire array. Cross-sectional scanning electron microscope (SEM) images of nanowires with diameters of (c) 50.3 ± 6.5 nm, (d) 70.0 ± 6.8 nm, (e) 107 ± 9.4 nm, (f) 155 ± 13 nm, and (g) 199 ± 19 nm. Nanowire lengths are consistently ∼425 nm (Figure S1). Scale bars are 500 nm.

To address these shortcomings, we employed a surface-cleaning step where a syringe pump dispensed a solution of dimethyl sulfoxide (DMSO) and chlorobenzene on the top of a rapidly rotating AAO template (Figure 1a-II). This solvent mixture dissolved the perovskite (as evidenced by a color change from dark red to transparent), removed residual material from the AAO surface, and drew liquid into the pores via capillary and centrifugal forces (Figure S2). Subsequent annealing led to perovskite recrystallization (returning to a dark red color) and nanowire formation at the bottoms of the pores. In this process, the high surface area at the pore bottom relative to the pore walls likely favors preferential nucleation and material growth at these locations. Because there is no chemical difference, we assume that the precursor materials crystallize similarly as they do within mesoporous scaffolds;[3] in this case, solid $CH_3NH_3PbI_3$ conforms to the cylindrical shape of the AAO pores and forms nanowires. Importantly, this synthetic procedure can be used to generate nanowire arrays over 80 cm² (Figure 1b) with uniform dimensions across the sample (Figure S3). To test whether this procedure is amenable to size control, templates with different pore diameters were then prepared (Figure S4). Indeed, $CH_3NH_3PbI_3$ nanowires ranging from D = 50–200 nm (Figure 1c–g) can be easily synthesized. Importantly, the dispersity in D was <10% for most samples, as determined by SEM (Figure 1).

To better understand the effect of D on crystallinity, each sample was characterized by XRD. These measurements confirmed that the target perovskite crystal structure was achieved for each of the nanowire samples (Figure S5). Subsequently, Williamson–Hall (WH) analysis was used to evaluate the relative crystallinity of each sample.[28] This analysis separates the contributions of lattice strain (ε_{WH}) and crystallite size to peak breadth. To perform this analysis, the full width at half-maximum[29] of five diffraction peaks characteristic of the $CH_3NH_3PbI_3$ perovskite crystal were plotted versus the diffraction angle (θ). For each sample, the data fit well to a linear model, as expected. Interestingly, D = 110 nm nanowires reproducibly exhibited the smallest absolute ε_{WH}, with greater ε_{WH} at both larger and smaller D (Figures 2a and S6). This property is consistent with reduced defect density, which is directly related to the rate of charge recombination.

In order to elucidate structure–function relationships in perovskite nanowires, time-resolved PL spectroscopy experiments were performed to analyze charge transport dynamics.[6] Decay curves were fit to a biexponential function such that two distinct populations of excited charge carriers (i.e., those that undergo fast surface recombination vs slow bulk recombination)[30] could be described.[31] For this comparative study, we report the overall characteristic lifetime (τ_c, which accounts for both populations of charge carriers) as a concise metric to evaluate charge transport within each nanowire sample (Figure 2b,c; Table S1). As expected from WH analysis, D = 110 nm exhibited the longest τ_c (∼60 ns), with reductions in τ_c observed with both increased and decreased D. The correlation between ε_{WH} and τ_c suggests that charge carrier lifetime is largely controlled by defect-driven lattice strain in these experiments (refer to the Supporting Information for additional discussion).

In order to demonstrate the general nature of this approach, perovskite nanowires with a variety of compositions were synthesized. In particular, halide substitution is known to
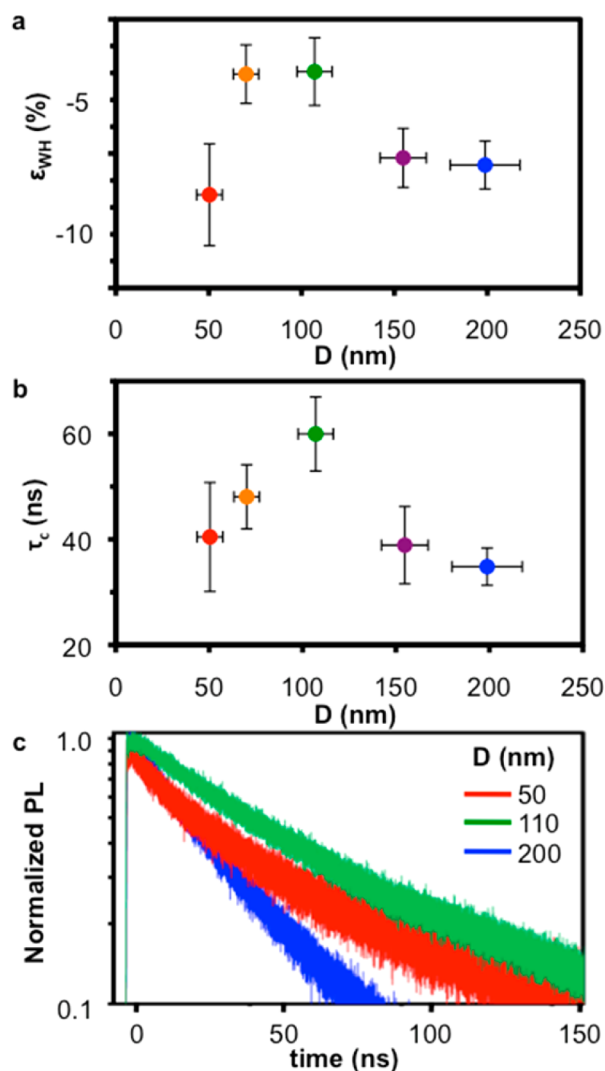
Figure 2. Structure−function relationships in $CH_3NH_3PbI_3$ nanowire arrays. (a) Estimated strain from WH analysis for different nanowire diameters (negative values signify lattice contraction). (b) Average τ_c for different nanowire diameters. (c) Representative PL decay curves.

Figure 3. Compositional generality in the templated synthesis of perovskite nanowires. Cross-section SEM images of (a) $CH_3NH_3PbBr_3$ and (b) Cs_2SnI_6 nanowires. Scale bars are 500 nm. (c) Powder XRD patterns of $CH_3NH_3PbBr_3$ and Cs_2SnI_6 nanowires.

enable bandgap tunability in organolead halide perovskites (~1.55−2.3 eV).[32] Use of the appropriate precursor solution and surface cleaning conditions indeed led to $CH_3NH_3PbBr_3$ nanowires with similar uniformity (Figure 3a). Beyond organolead halide perovskites, Cs_2SnI_6 has been investigated more recently as an inorganic, air-stable, lead-free alternative.[33,34] After the synthesis of Cs_2SnI_6 powder,[33] an analogous method was employed to deposit Cs_2SnI_6 nanowires from a single precursor solution (Figure 3b). XRD confirmed the expected crystal structures for both $CH_3NH_3PbBr_3$ and Cs_2SnI_6 nanowires (Figures 3c and S7), and to the best of our knowledge, Cs_2SnI_6 nanostructures have not been synthesized using any other method.

This work establishes a composition general method to synthesize perovskite nanowires with controlled diameter. Though a method of selective template dissolution is required for more advanced structural characterization (e.g., determining whether the nanowires are single crystalline), perovskite nanowires within AAO, which have not previously been reported for these compositions, are more uniform than those synthesized by other methods.[7,8,12,13,18] Additionally,
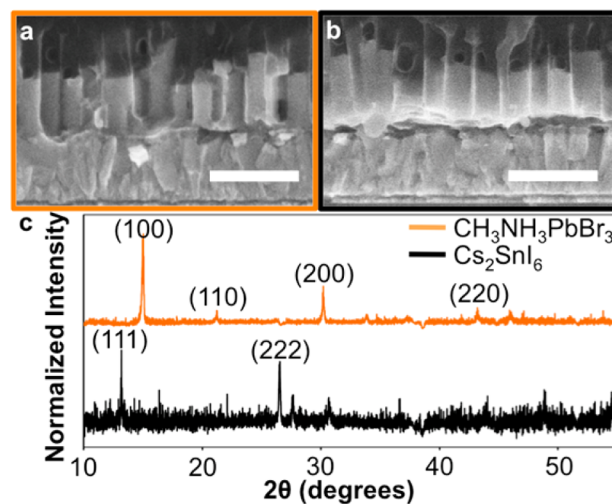
this technique does not require the use of unique ligands or surface chemistries for each new perovskite composition. The substrates used for synthesis (TiO_2/FTO-bound AAO) should enable a facile transition from fundamental nanowire characterization to array photovoltaic device fabrication because TiO_2, FTO, and AAO can act as a hole-blocking layer, transparent anode, and stabilizing scaffold, respectively, in an operational device. Thus, this establishes a route to perovskite-based, oriented nanowire array photovoltaics, which could be systematically modified in nanowire diameter, length, spacing, and composition to achieve optimal device performance.

■ ASSOCIATED CONTENT

ⓈSupporting Information
The Supporting Information is available free of charge on the ACS Publications website at DOI: 10.1021/jacs.6b05901.

    Materials and methods, additional SEM images describing AAO templates and the synthetic process, PXRD patterns, discussion of the biexponential PL decay fits, and Williamson-Hall plots (PDF)

■ AUTHOR INFORMATION

Corresponding Author
*chadnano@northwestern.edu
Notes
The authors declare no competing financial interest.

■ ACKNOWLEDGMENTS

■ REFERENCES

(1) Grätzel, M. *Nat. Mater.* **2014**, *13*, 838.

(2) Snaith, H. J. *J. Phys. Chem. Lett.* **2013**, *4*, 3623.

(3) Lee, M. M.; Teuscher, J.; Miyasaka, T.; Murakami, T. N.; Snaith, H. J. *Science* **2012**, *338*, 643.

(4) Liang, K.; Mitzi, D. B.; Prikas, M. T. *Chem. Mater.* **1998**, *10*, 403.

(5) Kojima, A.; Teshima, K.; Shirai, Y.; Miyasaka, T. *J. Am. Chem. Soc.* **2009**, *131*, 6050.

(6) Stranks, S. D.; Eperon, G. E.; Grancini, G.; Menelaou, C.; Alcocer, M. J.; Leijtens, T.; Herz, L. M.; Petrozza, A.; Snaith, H. J. *Science* **2013**, *342*, 341.

(7) Horváth, E.; Spina, M.; Szekrényes, Z.; Kamarás, K.; Gaal, R.; Gachet, D.; Forró, L. *Nano Lett.* **2014**, *14*, 6761.

(8) Zhu, H.; Fu, Y.; Meng, F.; Wu, X.; Gong, Z.; Ding, Q.; Gustafsson, M. V.; Trinh, M. T.; Jin, S.; Zhu, X. *Nat. Mater.* **2015**, *14*, 636.

(9) Eaton, S. W.; Lai, M.; Gibson, N. A.; Wong, A. B.; Dou, L.; Ma, J.; Wang, L.-W.; Leone, S. R.; Yang, P. *Proc. Natl. Acad. Sci. U. S. A.* **2016**, *113*, 1993.

(10) Xing, J.; Liu, X. F.; Zhang, Q.; Ha, S. T.; Yuan, Y. W.; Shen, C.; Sum, T. C.; Xiong, Q. *Nano Lett.* **2015**, *15*, 4571.

(11) Fu, Y.; Zhu, H.; Schrader, A. W.; Liang, D.; Ding, Q.; Joshi, P.; Hwang, L.; Zhu, X.; Jin, S. *Nano Lett.* **2016**, *16*, 1000.

(12) Im, J.-H.; Luo, J.; Franckevičius, M.; Pellet, N.; Gao, P.; Moehl, T.; Zakeeruddin, S. M.; Nazeeruddin, M. K.; Grätzel, M.; Park, N.-G. *Nano Lett.* **2015**, *15*, 2120.

(13) Zhu, F.; Men, L.; Guo, Y.; Zhu, Q.; Bhattacharjee, U.; Goodwin, P. M.; Petrich, J. W.; Smith, E. A.; Vela, J. *ACS Nano* **2015**, *9*, 2948.

(14) Kollek, T.; Gruber, D.; Gehring, J.; Zimmermann, E.; Schmidt-Mende, L.; Polarz, S. *Angew. Chem., Int. Ed.* **2015**, *54*, 1341.

(15) Fu, Y.; Meng, F.; Rowley, M. B.; Thompson, B. J.; Shearer, M. J.; Ma, D.; Hamers, R. J.; Wright, J. C.; Jin, S. *J. Am. Chem. Soc.* **2015**, *137*, 5810.

(16) Wong, A. B.; Lai, M.; Eaton, S. W.; Yu, Y.; Lin, E.; Dou, L.; Fu, A.; Yang, P. *Nano Lett.* **2015**, *15*, 5519.

(17) Zhu, P.; Gu, S.; Shen, X.; Xu, N.; Tan, Y.; Zhuang, S.; Deng, Y.; Lu, Z.; Wang, Z.-L.; Zhu, J. *Nano Lett.* **2016**, *16*, 871.

(18) Zhang, D.; Eaton, S. W.; Yu, Y.; Dou, L.; Yang, P. *J. Am. Chem. Soc.* **2015**, *137*, 9230.

(19) Martin, C. R. *Science* **1994**, *266*, 1961.

(20) Routkevitch, D.; Bigioni, T.; Moskovits, M.; Xu, J. M. *J. Phys. Chem.* **1996**, *100*, 14037.

(21) Lee, W.; Park, S.-J. *Chem. Rev.* **2014**, *114*, 7487.

(22) Qin, L.; Park, S.; Huang, L.; Mirkin, C. A. *Science* **2005**, *309*, 113.

(23) Ozel, T.; Ashley, M. J.; Bourret, G. R.; Ross, M. B.; Schatz, G. C.; Mirkin, C. A. *Nano Lett.* **2015**, *15*, 5273.

(24) Ozel, T.; Bourret, G. R.; Mirkin, C. A. *Nat. Nanotechnol.* **2015**, *10*, 319.

(25) Schierhorn, M.; Boettcher, S. W.; Kraemer, S.; Stucky, G. D.; Moskovits, M. *Nano Lett.* **2009**, *9*, 3262.

(26) Huang, J.; Jiang, K.; Cui, X.; Zhang, Q.; Gao, M.; Su, M.; Yang, L.; Song, Y. *Sci. Rep.* **2015**, *5*, 15889.

(27) Ball, J. M.; Lee, M. M.; Hey, A.; Snaith, H. J. *Energy Environ. Sci.* **2013**, *6*, 1739.

(28) Williamson, G.; Hall, W. *Acta Metall.* **1953**, *1*, 22.

(29) Zak, A. K.; Majid, W. A.; Abrishami, M. E.; Yousefi, R. *Solid State Sci.* **2011**, *13*, 251.

(30) Shi, D.; Adinolfi, V.; Comin, R.; Yuan, M.; Alarousu, E.; Buin, A.; Chen, Y.; Hoogland, S.; Rothenberger, A.; Katsiev, K.; et al. *Science* **2015**, *347*, 519.

(31) de Quilettes, D. W.; Vorpahl, S. M.; Stranks, S. D.; Nagaoka, H.; Eperon, G. E.; Ziffer, M. E.; Snaith, H. J.; Ginger, D. S. *Science* **2015**, *348*, 683.

(32) Noh, J. H.; Im, S. H.; Heo, J. H.; Mandal, T. N.; Seok, S. I. *Nano Lett.* **2013**, *13*, 1764.

(33) Lee, B.; Stoumpos, C. C.; Zhou, N.; Hao, F.; Malliakas, C.; Yeh, C.-Y.; Marks, T. J.; Kanatzidis, M. G.; Chang, R. P. *J. Am. Chem. Soc.* **2014**, *136*, 15379.

(34) Saparov, B.; Sun, J.-P.; Meng, W.; Xiao, Z.; Duan, H.-S.; Gunawan, O.; Shin, D.; Hill, I. G.; Yan, Y.; Mitzi, D. B. *Chem. Mater.* **2016**, *28*, 2315.